EUROPEAN ORGANIZATION FOR NUCLEAR RESEARCH


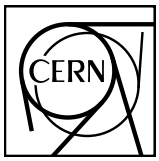


ALICE-PUBLIC-2021-005

# ALICE 2016-2017-2018 luminosity determination for pp collisions at $\sqrt{s}$ = 13 TeV

ALICE Collaboration*

**Abstract**

Luminosity determination in ALICE is based on the measurement of visible cross sections in van der Meer (vdM) scans. In the Run 2 (2015–2018), the Large Hadron Collider provided proton–proton collisions at a centre-of-mass energy of $\sqrt{s}$ = 13 TeV. One vdM scan per year was performed, which allowed for calibration of the ALICE luminometers: the T0 detector with pseudorapidity coverage $4.6 < \eta < 4.9$, $-3.3 < \eta < -3.0$, and the V0 detector with pseudorapidity coverage $2.8 < \eta < 5.1$, $-3.7 < \eta < -1.7$. This document presents the luminosity determination methodology and results for the years 2016, 2017 and 2018.



*See Appendix A for the list of collaboration members

## 1 Introduction

Luminosity determination in ALICE (A Large Ion Collider Experiment) [1] at the Large Hadron Collider (LHC [2]) is based on the measurement of visible cross sections in van der Meer (vdM) scans. The visible cross section $\sigma_{\rm vis}$ seen by a given detector (or set of detectors) with a given trigger condition is a fraction of the total inelastic interaction cross section $\sigma_{\rm inel}$: $\sigma_{\rm vis} = \varepsilon\sigma_{\rm inel}$, where $\varepsilon$ is the fraction of inelastic events that satisfy the trigger condition. In the following, a class of inelastic events satisfying a given trigger condition will be referred to as a reference process, and the detector providing the trigger signal will be referred to as a luminometer. Once the reference-process cross section ($\sigma_{\rm vis}$) is measured, the luminosity at the ALICE interaction point (IP2) is determined as the reference-process rate divided by $\sigma_{\rm vis}$. This procedure does not require a knowledge of $\varepsilon$.

The van der Meer (vdM) scan [3] is the most common technique employed for luminosity determination at colliders, see e.g. Ref. [4] for a review, and Refs. [5–12] for measurements performed at the LHC. In vdM scans, the two beams are moved across each other in the $x$ (horizontal) and $y$ (vertical) directions. The rate $R(\Delta x, \Delta y)$ of the reference (visible) process is measured as a function of the transverse beam separations $\Delta x$ and $\Delta y$, defined as the distance between the centroids of the beam bunches. The procedure allows one to determine the luminosity $L$ for head-on collisions of a pair of bunches with particle intensities $N_1$ and $N_2$ as

$$L = N_1 N_2 f_{\rm rev}/(h_x h_y), \tag{1}$$

where $f_{\rm rev}$ is the accelerator revolution frequency and $h_x$ and $h_y$ are the effective convolved beam widths in the two transverse directions. $h_x$ and $h_y$ are measured as the area below the $R(\Delta x, 0)$ and $R(0, \Delta y)$ curve (scan area), respectively, each divided by the head-on rate $R(0,0)$. The cross section $\sigma_{\rm vis}$ for the chosen reference process is then

$$\sigma_{\rm vis} = R(0,0)/L. \tag{2}$$

The standard vdM scans are typically coupled with a length-scale calibration scan, whose aim is to determine the global conversion factor from the nominal beam displacement (as dialled by the accelerator operator) to the actual one. In these scans, the two beams are kept at constant separation and moved in consecutive steps in the same direction, and the position of the interaction vertex is measured as a function of the nominal beam position.

The vdM formalism assumes complete factorisation of the beam profiles in the two transverse directions, such that the beam overlap region is fully described by the product $h_x h_y$. Previous studies performed by ALICE [11, 13–17] and other LHC experiments [6, 7, 9, 18] have shown that the actual LHC bunch shapes can violate the factorisation assumption. The size of the effect was found to vary from scan to scan and demanded corrections ranging from the per mil to the percent level. Non-factorisation effects can be studied and quantified by measuring the luminous region parameters, via the distribution of interaction vertices, as a function of the beam separation.

In the Run 2 (2015–2018), the LHC provided proton–proton (pp) collisions at a centre-of-mass energy of $\sqrt{s}$ = 13 TeV. The luminosity determination for the year 2015 is discussed in Ref. [13]. This document presents the ALICE luminosity determination and methodology for the years 2016, 2017, and 2018. For each of these years, a van der Meer scan was performed and the cross section was measured for two reference processes. In Sec. 2 the detectors used for the measurement are briefly described, along with the relevant machine parameters and the adopted scan procedure. In Sec. 3 the vdM scan analysis procedure is described and the results and uncertainties for the visible cross section and the luminosity measurement are presented and discussed.

**Table 1:** Running conditions for the 2016, 2017, and 2018 vdM scans. The solenoid (dipole) field is parallel to the $z$ ($x$) axis of the ALICE coordinate system. A positive crossing angle implies that the two beams exit the crossing region with positive $y$ coordinate with respect to the beam axis.

| Year | 2016 | 2017 | 2018 |
|---|---|---|---|
| Date | May 17 | July 27 | June 30 |
| LHC fill | 4937 | 6012 | 6864 |
| Bunches per beam | 55 | 57 (beam 1), 56 (beam 2) | 70 |
| Colliding bunch pairs at IP2 | 28 | 20 | 20 |
| Average bunch intensity ($10^{10}$ p) | $\sim$ 7 | $\sim$ 8 | $\sim$ 9 |
| $\beta^*$ (m) | 19 | 19 | 19 |
| Nominal vertical half crossing angle ($\mu$rad) | +85 | +70 | +70 |
| ALICE solenoid/dipole field (T) | +0.5/−0.7 | +0.5/−0.7 | +0.5/−0.7 |

## 2 Experimental setup

In the vdM scans, the cross section was measured for two reference processes: one is based on the V0 detector, the other on the T0 detector. A detailed description of these detectors is given in Ref. [1], and their performance is discussed in Refs. [19–21]. The V0 detector consists of two hodoscopes, with 32 scintillator tiles each, located on opposite sides of the LHC interaction point 2 (IP2), at distances of 340 cm (V0A) and 90 cm (V0C) along the beam axis, covering the pseudorapidity ($\eta$) ranges $2.8 < \eta < 5.1$ (V0A) and $-3.7 < \eta < -1.7$ (V0C). The T0 detector consists of two arrays of 12 Cherenkov counters each, located on opposite sides of IP2, at distances of 370 cm (T0A) and 70 cm (T0C) along the beam axis, covering the pseudorapidity ranges $4.6 < \eta < 4.9$ (T0A) and $-3.3 < \eta < -3.0$ (T0C). Note that the clockwise-travelling LHC beam moves from side A to side C.

The V0-based trigger condition, chosen as the reference process, requires at least one hit in each detector hodoscope, i.e. on both sides of IP2. A similar trigger condition defines the T0-based reference process, with the additional condition that the longitudinal coordinate of the interaction vertex lies in the range $|z| < 30$ cm, where $z = 0$ is the nominal IP2 position [1]. More details on this online selection, which rejects the background from beam–gas and beam–satellite interactions, are given in Ref. [13].

The analysis procedure uses, for the length-scale calibration and non-factorisation corrections, the parameters of the luminous region measured via the distribution of interaction vertices, determined with the ALICE Inner Tracking System (ITS [22]).

Table 1 reports, along with the date and LHC fill [2] number for each scan, the main parameters defining the scan conditions, namely: total and colliding bunches, typical bunch intensities, $\beta^*$ [3], crossing angle, and fields in the ALICE magnets. In all scans, the minimum spacing between two consecutive colliding bunch pairs at IP2 was 1 $\mu$s.

The maximum beam separation during the scan was about 0.6 mm, corresponding to about six times the RMS of the transverse beam profile ($\sigma_{\text{beam}}$). The reference-process rates were recorded (and the cross section measured) separately for each colliding bunch pair. Two statistically independent measurements per bunch pair were performed by repeating the (horizontal and vertical) scan pair twice. In addition,

[1] ALICE uses a Cartesian system whose origin is at IP2. The $z$ axis is parallel to the mean beam direction at IP2 and points along the LHC Beam 2 (i.e. LHC anticlockwise). The $y$ axis points upwards, while the $x$ axis is perpendicular to the $y$ and $z$ axes, forming a right-handed orthogonal system.

[2] A fill is a time interval with continued presence of beam in the accelerator; it starts with the injection and ends with the beam dump.

[3] The $\beta(z)$ function describes the single-particle motion and determines the variation of the beam envelope as a function of the coordinate along the beam orbit ($z$). The transverse size of the beam at a given position along the beam trajectory is proportional to the square root of $\beta$. The notation $\beta^*$ denotes the value of the $\beta$ function at the interaction point.

**Table 2:** Obtained values for a number of parameters and correction factors mentioned in the text, for the 2016, 2017, and 2018 vdM scans. The uncertainties on the $\alpha$ and $\beta$ parameters are statistical. The origin of the uncertainties on the other quantities is discussed in the text.

| | 2016 | 2017 | 2018 |
|---|---|---|---|
| Ghost-charge correction factor | $0.99707 \pm 0.00014$ | $0.9987 \pm 0.0002$ | $0.9987 \pm 0.0003$ |
| $\alpha_{\mathrm{T0}}$ | $0.4459 \pm 0.0001$ | $0.4990 \pm 0.0002$ | $0.4900 \pm 0.0002$ |
| $\beta_{\mathrm{T0}}$ | $0.3912 \pm 0.0001$ | $0.3933 \pm 0.0002$ | $0.4005 \pm 0.0002$ |
| $\alpha_{\mathrm{V0}}$ | $0.07600 \pm 0.00003$ | $0.07703 \pm 0.00004$ | $0.07684 \pm 0.00004$ |
| $\beta_{\mathrm{V0}}$ | $0.06137 \pm 0.00003$ | $0.06216 \pm 0.00004$ | $0.06193 \pm 0.00004$ |
| Length-scale calibration factor ($x$) | $1.010 \pm 0.002$ | $1.013 \pm 0.002$ | $1.012 \pm 0.002$ |
| Length-scale calibration factor ($y$) | $1.007 \pm 0.001$ | $1.011 \pm 0.002$ | $1.003 \pm 0.002$ |
| Non-factorisation correction factor | $1.005 \pm 0.005$ | $1.002 \pm 0.002$ | $1.004 \pm 0.004$ |

a length-scale calibration scan was performed. Finally, a vdM scan with non-zero separation (offset) in the non-scanned direction was performed, to provide additional input for non-factorisation studies. The offset amounts to about 2 $\sigma_{\mathrm{beam}}$.

The bunch-intensity measurement is provided by the LHC instrumentation [23]: a DC current transformer (DCCT), measuring the total beam intensity, and a fast beam current transformer (fBCT), measuring the relative bunch populations. For the relative bunch intensities, data from a second device, the ATLAS beam pick-up system (BPTX [24]) was also used. The measured beam intensity was corrected for the fraction of ghost and satellite charge. The accelerator orbit is nominally divided in 3564 slots of 25 ns each. Given the radio-frequency configuration of the LHC, each slot is divided in ten buckets of 2.5 ns each. In nominally filled slots, the so-called main bunch is captured in the central bucket of the slot. Following the convention established in Ref. [25], the charge circulating outside of the nominally filled slots is referred to as ghost charge; the charge circulating within a nominally filled slot but not captured in the central bucket is referred to as satellite charge. The ghost and satellite charge do not contribute to the luminosity at the nominal interaction point, hence they must be subtracted from the total beam intensity. A measurement of the ghost-charge fraction was provided independently by the LHC Longitudinal Density Monitor (LDM), which measures synchrotron radiation photons emitted by the beams [26], and by the LHCb collaboration, via the rate of beam–gas collisions occurring in nominally empty bunch slots, as described in Refs. [9, 27]. The measured ghost-charge correction factors to the bunch-intensity product $N_1N_2$ are shown, for all scans, in Table 2. The LDM provides in addition a measurement of the satellite-charge fraction, which was found to be negligible ($< 0.05\%$) for all scans.

## 3 Analysis and results

Three steps are needed to convert the raw T0 and V0 trigger rates into the actual reference process rates.

First, the contamination by beam–satellite and beam–gas interactions in the V0 rate is removed using the detector timing measurements. The background is identified via the sum and difference of arrival times in the two V0 arrays from offline analysis of the data collected during the scan [11, 19]. The arrival times are obtained by averaging over the signal times of all hits of each array. The background contamination is measured as the fraction of events in which the sum and difference of times lie outside of a window of $\pm 3$ ns around the values expected for beam–beam collisions. The measurement is performed for each separation value and the corresponding raw rate is corrected by the obtained fraction. This procedure has only a small effect ($< 1\%$) when applied to the T0 rates, due to the vertex cut in the T0 trigger logic described in Sec. 2. In order to study a possible contamination of the trigger rate by the intrinsic noise counts of the detectors, the rate of both trigger signals in the absence of beam was measured and found

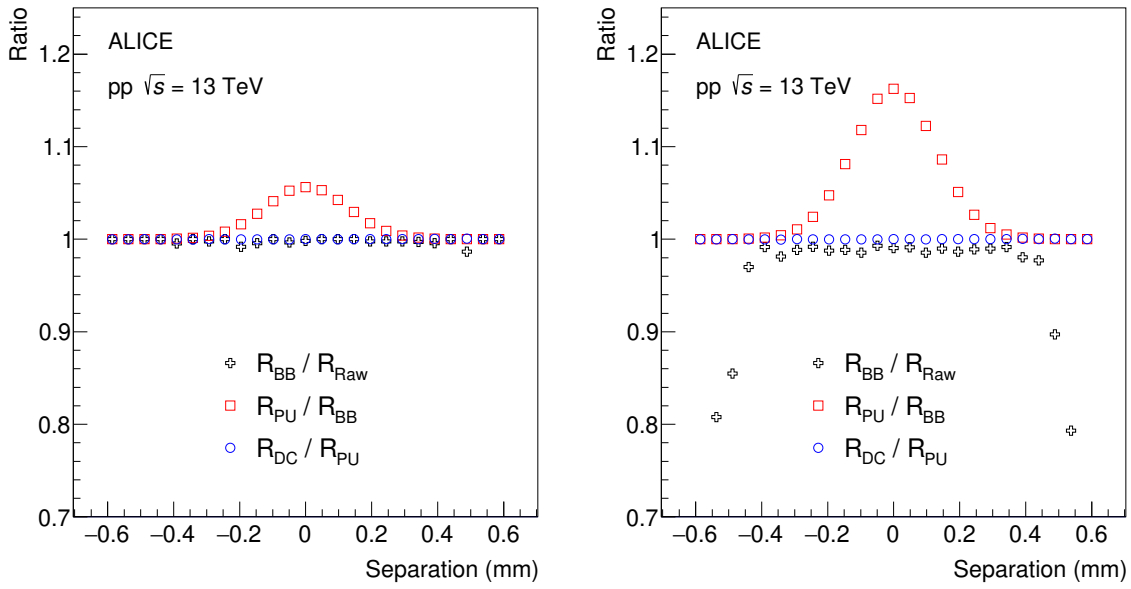


**Fig. 1:** Relative modification of the T0 (left) and V0 (right) trigger rate after background ($R_{BB}/R_{raw}$), pile-up ($R_{PU}/R_{BB}$) and luminosity decay ($R_{DC}/R_{PU}$) are taken into account, as a function of the beam separation, for one typical pair of colliding bunches during the first 2016 horizontal scan.

to be zero. The rate in empty bunch slots with beam circulating was also measured and found to be zero for the T0. For the V0, a significant counting rate was measured in the slots immediately after a filled one, due to after-pulses. However, the rate in empty slots immediately preceding a filled one is smaller by a factor of about $10^{-5}$ than that in filled slots, pointing to a negligible after-pulse effect on the rate measurement.

Second, the probability of multiple interactions in the same bunch crossing (pile-up) is taken into account according to Poisson statistics. Since both reference processes consist of a coincidence of hits on the A and C sides, their measured rate after background subtraction ($R_{BB}$) is given, for a given bunch pair, by

$$R_{BB} = f_{rev} \{1 - \exp(-\mu_{vis}) + \exp(-\mu_{vis}) [1 - \exp(-\mu_{AnotC})] [1 - \exp(-\mu_{CnotA})]\} \quad (3)$$

where $\mu_{vis} = L\sigma_{vis}/f_{rev}$ is the average number of genuine coincidences (i.e. of visible interactions) per bunch crossing and $\mu_{AnotC}$ ($\mu_{CnotA}$) is the average number of pp collisions per bunch crossing resulting in a hit on the A (C) side only. The ratios $\alpha = \mu_{AnotC}/\mu_{vis}$ and $\beta = \mu_{CnotA}/\mu_{vis}$ were obtained by setting up dedicated one-arm triggers (V0A&!V0C and V0C&!V0A, and similarly for T0), and performing a $\chi^2$ minimisation fit to their measured rates at different scan steps. The obtained values for $\alpha$ and $\beta$ are shown, for both T0 and V0, in Table 2. Knowledge of $\alpha$ and $\beta$ allows one to retrieve the value of $\mu_{vis}$ from the measured $R_{BB}$, by numerically inverting Eq. 3. The pile-up-free process rate is then given by $R_{PU} = f_{rev}\mu_{vis}$.

Finally, a correction is performed to account for the bunch intensity (and, hence, the luminosity) decay with time. The rates at each separation [4] are rescaled by the ratio of the corresponding bunch intensities to the bunch intensities at an arbitrary timestamp ($t_0$), chosen to lie between the horizontal and vertical scan.

As an example, the relative modification of the rate after each of the three above-described steps is shown

[4] The acquisition time for each separation value is 30 s, negligible with respect to the half-life of the beam, which is typically of a few hours

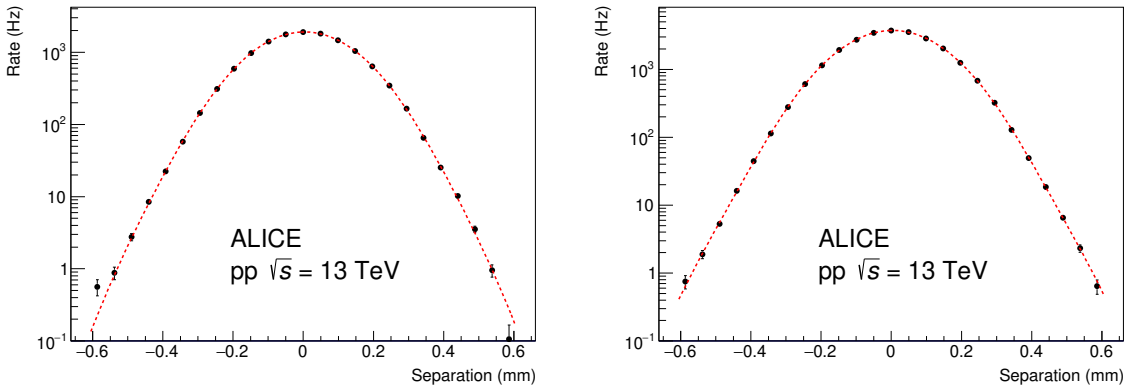


**Fig. 2:** Rates of the T0 (left) and V0 (right) reference processes as a function of beam separation for one typical pair of colliding bunches in the first 2016 horizontal vdM scan. The solid red curve is a fit according to Eq. 4.

for one bunch pair, as a function of the beam separation, in Fig. 1.

The measured scan curves are also corrected for orbit drifts, i.e. variations in time of the reference beam orbit, leading to a difference between the nominal and the actual beam separation. In order to quantify the bias, the data from the LHC Beam Position Monitors (BPM) [28] in various locations along the ring are used to extrapolate the transverse coordinates of the reference orbit of the two beams at IP2, for each scan step, using the YASP steering program [29]. Due to leakage of the (nominally closed) orbit bumps induced by the corrector magnets used for the vdM scan, the BPM data collected during the scan cannot be used for such a procedure, since they are themselves affected by the scan features. Hence, data was collected in between and outside scans, and their time-dependence was fitted with a polynomial function, which was then used to interpolate the reference orbit position of each beam during the scan, and to determine the correction to their separation, which is typically at the $\mu$m level.

The scan curves are corrected for beam–beam effects, which include both mutual repulsion (beam–beam deflection [30]) and (de-)focusing (optical distortion). The beam–beam deflection affects the beam separation, while the optical distortion affects the luminosity, hence the rate. These effects are corrected for using the framework outlined in Ref. [31]. The corrections depend on the separation, on the bunch pair intensities, on the effective beam widths $h_{\mathrm{x}}$ and $h_{\mathrm{y}}$ [5], and on the accelerator optics parameters (betatron tunes $Q_x$ and $Q_y$, $\beta^*$). The corrections for the separation are at the $\mu$m level, while those for the luminosity are at the percent level.

Once the corrections described above are applied, the scan curves are fitted, to determine the effective beam widths $h_x$ and $h_y$. It was found that the scan curves $R(\Delta x,0)$ and $R(0,\Delta y)$ are satisfactorily described by a Gaussian function multiplied by a symmetric sixth-order polynomial function:

$$R(\Delta x,0) = R(\mu,0)\exp\left[-(\Delta x-\mu)^2/2\sigma^2\right]\left[1+p_2(\Delta x-\mu)^2+p_4(\Delta x-\mu)^4+p_6(\Delta x-\mu)^6\right], \quad (4)$$

and similarly for $R(0,\Delta y)$. $R(\mu,0)$, $\mu$, $\sigma$, $p_2$, $p_4$ and $p_6$ are fit parameters. The $\mu$ parameter accounts for a possible mismatch between the nominal and the actual head-on position. The $\chi^2/ndf$ value of the fit is $\sim 1$ on average, and typically $\leq 2$. As an example, the fitted curves for one bunch pair are shown in Fig. 2.

The measured beam widths are corrected by a length-scale calibration factor, as discussed in Sec. 1. The calibration is performed in a dedicated run, where the two beams are moved simultaneously in the same direction in steps of equal size; the changes in the primary interaction vertex position provide a

[5] The beam widths used for this step are obtained from a preliminary analysis where orbit drift alone is taken into account. It was checked that such an approximation has a negligible effect on the obtained values.

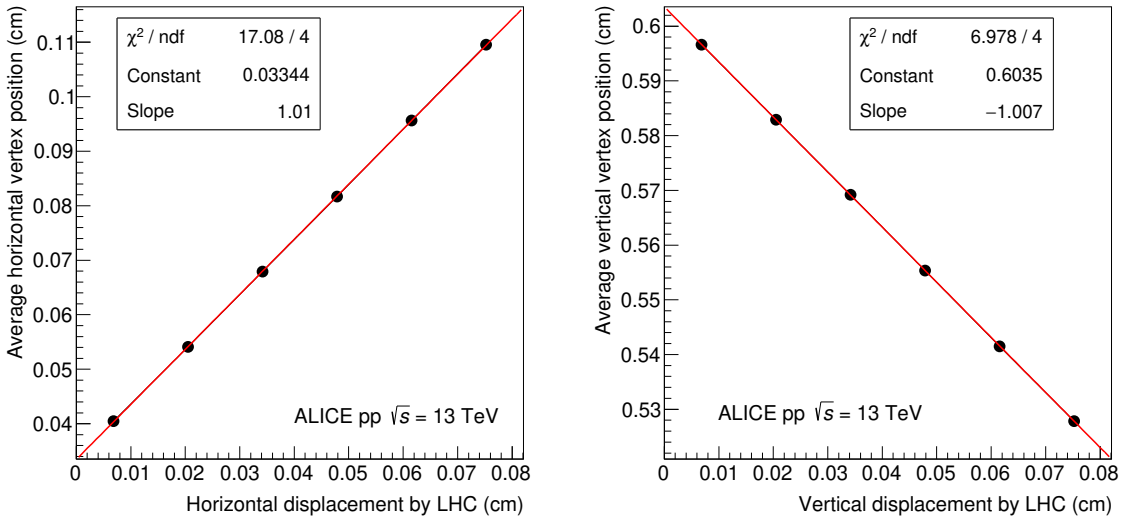


**Fig. 3:** Average horizontal (left) and vertical (right) vertex coordinate as a function of the nominal beam displacement in the 2016 length-scale calibration run, with superimposed linear fit (solid red line).The error bars are smaller than the marker size.

measurement of the actual beam displacement, which is used to extract a correction factor to the nominal displacement scale. The vertex position is measured using tracks reconstructed in the ALICE Inner Tracking System [22]. For each step, the vertex position and its uncertainty are obtained from a Gaussian fit to the vertex distribution. The length-scale correction factor is the slope parameter of a linear fit to the measured vertex displacement as a function of the nominal displacement (Fig. 3). Since this correction affects the global beam-displacement scale, the effective beam widths $h_x$ and $h_y$ are multiplied by their respective correction factors, shown in Table 2.

The possible presence of non-factorisation effects is assessed using the method proposed in Ref. [32] and briefly summarised in the following. First, the three-dimensional vertex distribution is measured, using the ITS, for each separation step during the standard and offset scans, and used to determine the luminous region parameters, namely: its mean position; its RMS size along the three spatial directions; and its transverse tilt ($x$–$y$ covariance). Deconvolution of the finite detector resolution for vertex determination is performed with the method described in Ref. [33]. As an example, the measured parameters for one of the scans are shown, as a function of separation, in Fig. 4. Second, the evolution of the luminous region parameters and of the reference process rates with separation is simultaneously fitted according to a model assuming that the probability density function of particles in a bunch is a three-dimensional non-factorisable double Gaussian. Data from all scans are fitted together. The model, shown as a solid line in Fig. 4, is able to reproduce the main features of the evolution with separation of the luminous region parameters. Third, the obtained fit parameters are used to compute, within the same model, the luminosity for head-on beams, which is then compared to that obtained with Eq. 1. The resulting correction factors, integrated over all colliding bunch pairs, are shown in Table 2. They are defined as the ratio of the head-on luminosities given by the model without and with the factorisation assumption. They enter the analysis as a multiplicative factor to $\sigma_{\rm vis}$. Since the correction relies on recorded ITS data, the sample size was limited by the acquisition dead time. Hence, a statistically significant bunch-by-bunch measurement of the correction factor could not be performed. It was however checked that the results for those bunch pairs for which the measurement is feasible are all compatible among themselves and with the integrated result.

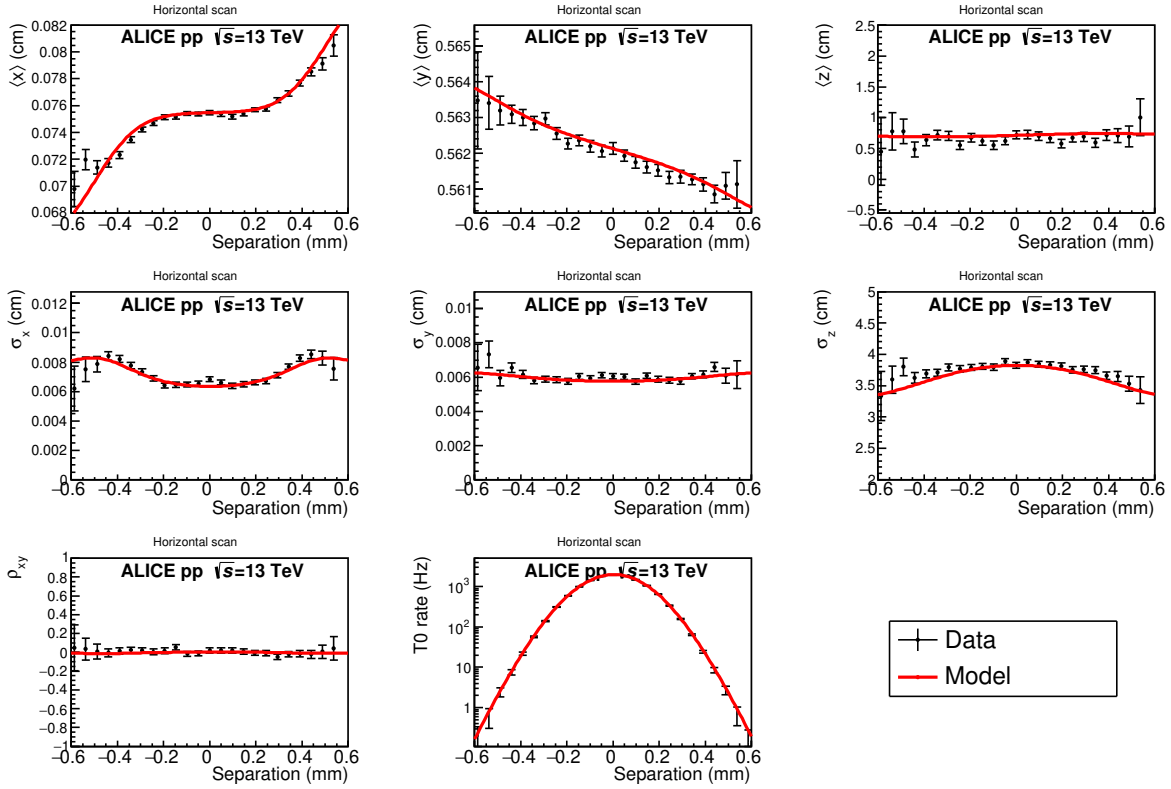


**Fig. 4:** Luminous region parameters and T0 rate as a function of separation during a horizontal vdM scan taken in 2016, as fitted by a three-dimensional correlated model [32] (solid red line). The centroids are shown in the top row, the RMS sizes are shown in the middle row, and the transverse tilt is shown in the bottom row together with the T0 rate.

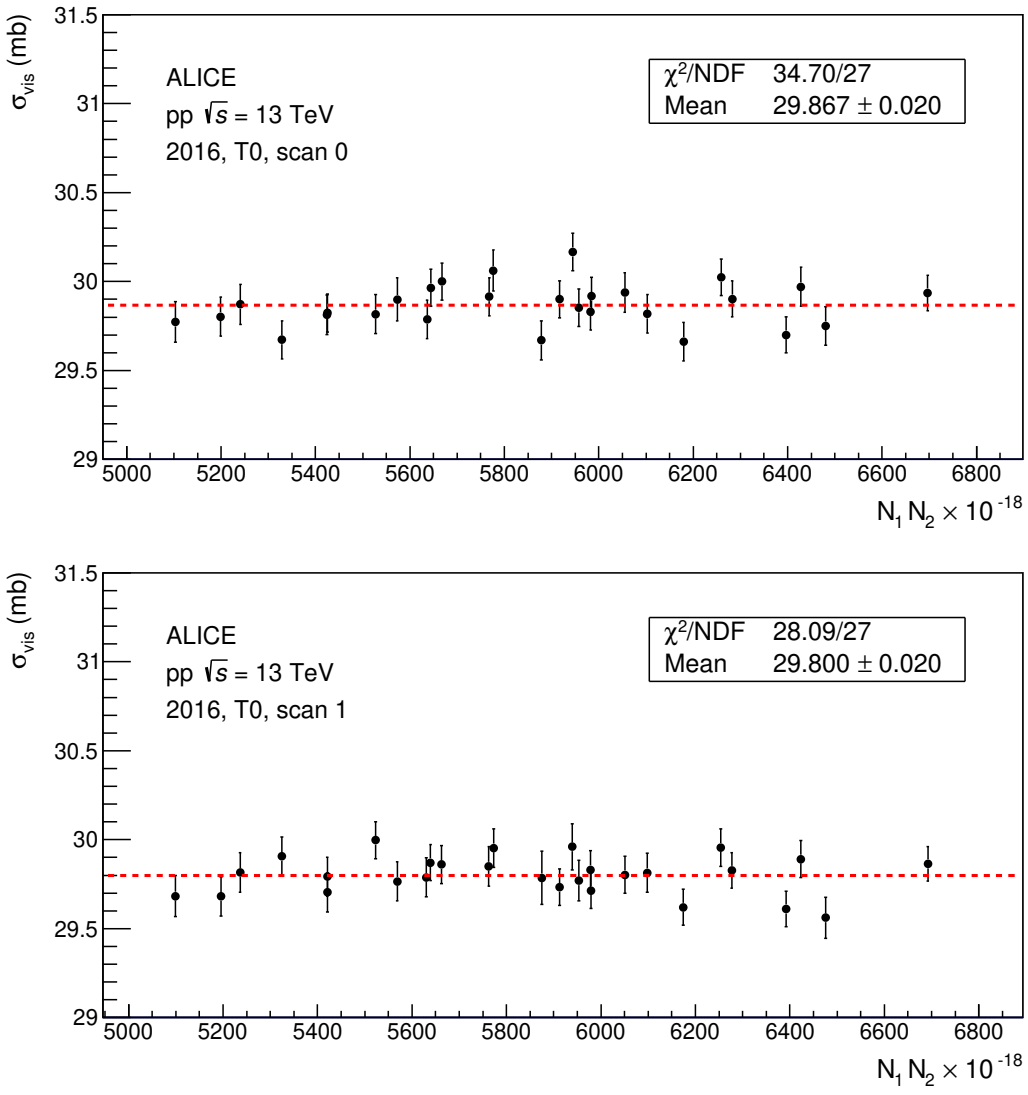


**Fig. 5:** Visible cross section for the T0 measured in the first (top) and second (bottom) 2016 vdM scan, as a function of the product of the intensities of the colliding bunch pair. Only the statistical uncertainties are shown. The solid line is a zero-order-polynomial fit to the data.

The cross section for each colliding bunch pair [6] and reference process is calculated according to Eq. 1 and 2 from the measured bunch intensities, from the beam widths and head-on rates obtained from the fit to the scan curves, and applying the length-scale and non-factorisation corrections. As there are two measured head-on rates per scan pair (one from the vertical and one from the horizontal scan), the arithmetic mean of the two is used.

As an example, the measured visible cross sections for the T0-based (V0-based) reference process in the two scans are shown in Fig. 5 (Fig. 6) for all the colliding bunch pairs of the 2016 vdM scan, as a function of the product $N_1N_2$ of the colliding bunch intensities. No significant dependence of the results on $N_1N_2$ is observed for any of the scans.

For both processes, and for the two scans, the weighted average of results from all colliding bunch pairs is computed (Figs. 5 and 6). The weighted average of the results of the two scans is retained as the final

[6] For the 2017 vdM scan, 8 colliding bunch pairs showed emittance instabilities and had to be discarded from the analysis.

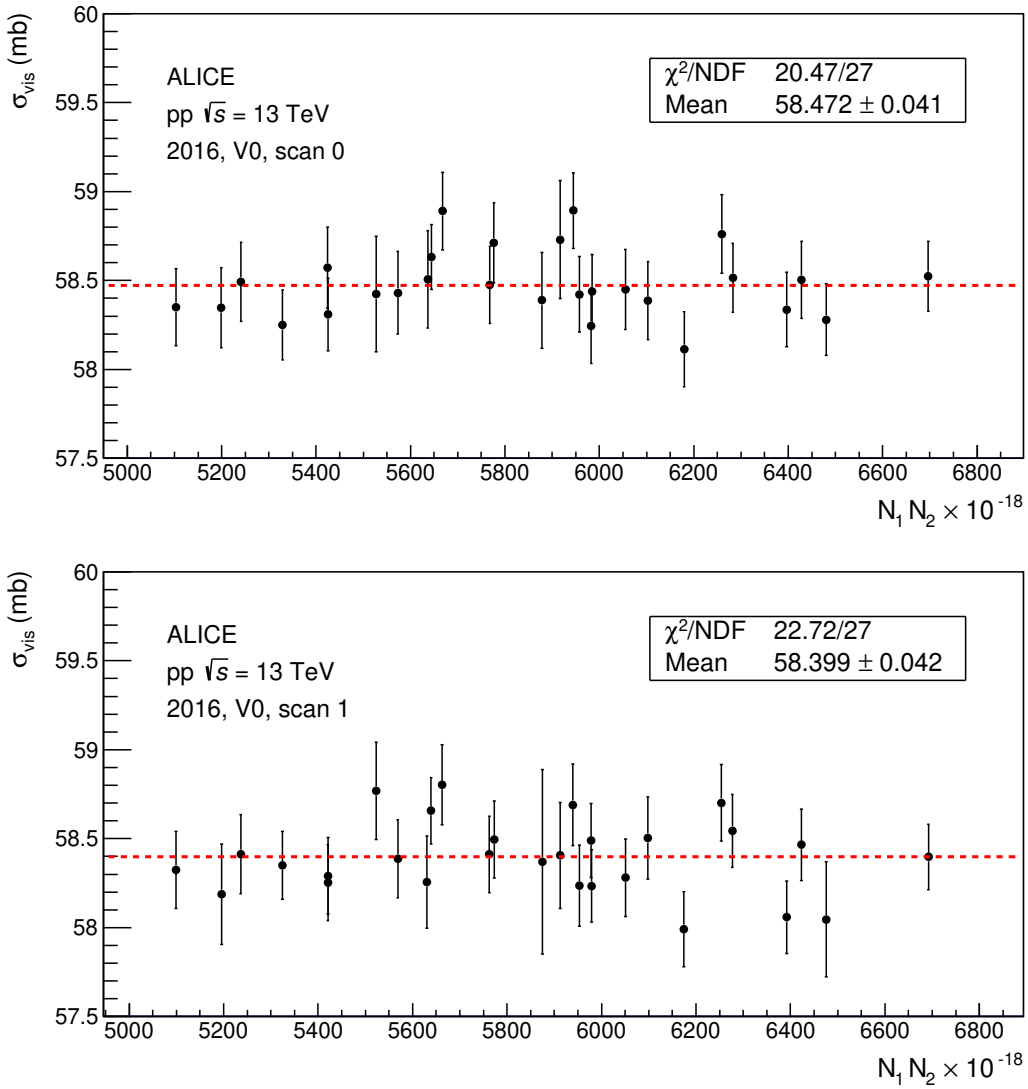


**Fig. 6:** Visible cross section for the V0 measured in the first (top) and second (bottom) 2016 vdM scan, as a function of the product of the intensities of the colliding bunch pair. Only the statistical uncertainties are shown. The solid line is a zero-order-polynomial fit to the data.

**Table 3:** Visible cross sections for the T0- and V0-based reference processes in the 2016, 2017, and 2018 vdM scans. Only the statistical uncertainties are reported.

| | 2016 | 2017 | 2018 |
|---|---|---|---|
| $\sigma_{\mathrm{T0}}$ (mb) | $29.838 \pm 0.015$ | $28.49 \pm 0.02$ | $28.159 \pm 0.014$ |
| $\sigma_{\mathrm{V0}}$ (mb) | $58.44 \pm 0.03$ | $58.10 \pm 0.04$ | $57.52 \pm 0.03$ |

result. The measured visible cross sections are reported in Table 3. The combined effect of beam–beam deflection and optical distortions on the measured cross sections is on the order of 0.8–1%, while that of orbit drift is on the order of 0.1–0.2%.

The sources of systematic uncertainty considered are listed below.

- Bunch intensity: the uncertainty on the bunch-intensity product $N_1N_2$ has three components: the uncertainty on the absolute DCCT calibration, evaluated as outlined in Ref. [34]; the uncertainty on the relative bunch populations, evaluated as the difference between the results obtained using the fBCT and the ATLAS BPTX; and the uncertainty on the ghost-charge correction, which includes the statistical and systematic uncertainties on the LDM measurement (as discussed in Ref. [26]) and, as the dominant contribution, the difference between the LDM and the LHCb measurements.
- Non-factorisation: an uncertainty of the same size as the applied correction is assigned to this effect.
- Length-scale calibration: the uncertainty on the scale factor reported in Table 2 is that from the linear fit to the measured vertex displacement (see e.g. Fig. 3), re-scaled by $\sqrt{\chi^2/ndf}$, to account for possible non-linearities during the length-scale calibration scan. The resulting uncertainty on the visible cross section is the quadratic sum of the uncertainties on the horizontal and vertical scale factors.
- Beam–beam effects: the corrections for beam–beam deflection and optical distortions have been recomputed after varying the beam optics parameters within their typical uncertainties: $\pm$ 0.002 units for the betatron tunes, $\pm$ 10% for $\beta^*$, conservatively assuming full correlation between the two beams and directions. In addition, the magnitude of a possible tune shift due to collisions in other LHC interaction points during the ALICE vdM scan has been estimated. The difference with respect to the cross section obtained with nominal values is quoted as uncertainty. The three contributions (tunes, $\beta^*$ and tune shift) are treated independently, and the corresponding uncertainties are summed in quadrature.
- Orbit drift: an uncertainty of the same size as the effect of the correction is assigned to this effect.
- Magnetic non-linearity: possible non-linearities in the steering magnet behaviour during the vdM scan, e.g. due to hysteresis, were considered as a source of systematic uncertainty. A preliminary hysteresis model [7] developed for the LHC was used to obtain an upper limit for the variations with respect to the nominal separation at each scan step; the variations where propagated to the cross section, and the difference with respect to the nominal value is quoted as an uncertainty.
- Beam centring: the measurement of the head-on rate $R(\mu, 0)$ in the horizontal scan can be affected by a non-optimal alignment of the two beams in the vertical direction, and vice versa. For each scan direction, such a misalignment is quantified via the $\mu$ parameter of Eq. 4 obtained for the other direction. The effect on the measured head-on rates, estimated using Eq. 4, is quoted as a systematic uncertainty.

[7] M. Hostettler and E. Todesco, 2020, presentations at the LHC Luminosity Calibration and Monitoring Working Group, November 16, and 2021, private communication, April 24.

- Luminosity decay: the bias arising from the variations in time of the head-on luminosity (expected from intensity burn-off, emittance growth and, possibly, a residual orbit-drift effect) is estimated via the difference between the head-on rates measured in the horizontal and vertical scans.

- Background subtraction: in order to evaluate a possible bias arising from beam–beam events identified as beam–gas by the criteria described earlier, the analysis has been repeated by increasing the width of the window for beam–beam events from 6 to 12 ns. The difference with respect to the cross section obtained with the nominal window size is quoted as uncertainty.

- Pile-up: the analysis has been repeated by varying the $\alpha$ and $\beta$ parameters within a conservative 10% uncertainty. For all fills the effect on the cross section is less than 0.2% for T0, and negligible ($\ll 0.1\%$) for V0. It is quoted as an uncertainty for the 2016 and 2018 scans. When comparing the ratio $\sigma_{\mathrm{T0}}/\sigma_{\mathrm{V0}}$ measured in the 2017 vdM scan (where, for head-on beams, $\mu_{\mathrm{vis}} \sim 0.4$ for V0) to the average ratio between the T0 and V0 rates measured at low interaction rate ($\mu_{\mathrm{vis}} \sim 0.001$–$0.05$ for V0) in the same LHC fill as the vdM scan, a difference of about 0.7% is observed. To account for such a discrepancy of the ratio, a systematic uncertainty, computed as the measured relative difference divided by $\sqrt{2}$, is assigned to both cross sections for this scan.

- Fit-model dependence: the analysis has been repeated by using numerical integration of the scan curve (see Ref. [11] for details) instead of a fit. The difference with respect to the result obtained with the fit is quoted as uncertainty.

- Consistency of the measured beam widths: since the effective beam widths are independent of the process used to measure them, a consistency check is performed by computing the ratio of the $h_x h_y$ quantities of Eq. 1 obtained with the T0 and the V0 for each colliding bunch. The bunch-pair-averaged difference between the $h_x h_y$ quantities measured with the T0 and the V0 is quoted as an uncertainty.

- Bunch-by-bunch consistency: in order to account for non-statistical bunch-by-bunch fluctuations of the measured cross section, a systematic uncertainty of $\sqrt{\chi^2/ndf - 1}$ times the statistical uncertainty of the weighted average is considered, where $\chi^2/ndf$ refers to a constant-value fit such as those of Fig. 5 and 6.

- Scan-to-scan consistency: the difference between the bunch-pair-averaged results from the two scans, when not compatible with the statistical uncertainties, is assigned as a systematic uncertainty.

Combining all the above-mentioned uncertainties, one obtains a total systematic uncertainty on the visible cross section ranging from 1.0% to 1.4%, depending on the year and luminometer.

During 2016, 2017, and 2018, ALICE collected data under varying conditions, depending on the beam configuration and the trigger strategy. The typical running conditions foresee a V0 rate of 100–150 kHz, with a minimum spacing between collisions of 25 ns and $\mu_{\mathrm{vis}} \sim 0.005$–$0.01$. For a number of special runs, data were taken at larger $\mu_{\mathrm{vis}}$, up to $\sim 0.05$.

In order to test the stability of the luminosity measurement provided by the T0 and the V0 throughout the considered running period, the ratio between the T0- and the V0-based luminosities has been computed for all recorded runs [8].

The reference process rates are determined from the raw rates with the same procedure used in the vdM scan, and divided by their respective cross sections to find the luminosity. In order to suppress the

[8] In the ALICE nomenclature, a run is a set of data collected within a start and a stop of the data acquisition, under stable detector and trigger configuration. Run durations range from a few minutes to several hours.

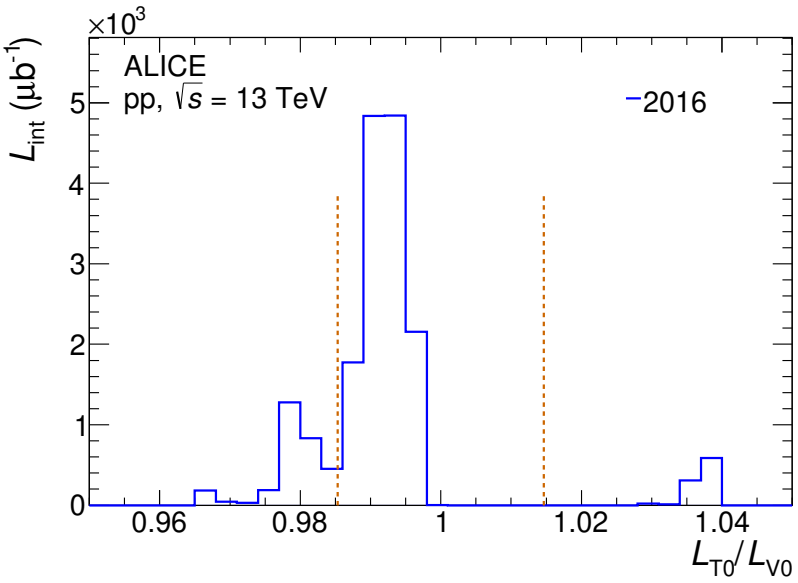


**Fig. 7:** Distribution of the ratio between the T0- and V0-based luminosities for all runs in 2016, weighted with the run integrated luminosity $L_{\rm int}$; the dashed vertical lines are located at $L_{\rm T0}/L_{\rm V0} = 1 \pm \delta$, where $\delta$ is the mean quadratic difference from unity.

bias induced by after-pulses on the V0 rates for dense filling schemes, the raw rates are measured after the data-acquisition system veto and corrected for dead time. The distribution of the luminosity ratio, weighted by the run integrated luminosity, is computed for each year, as shown in Fig. 7. The mean quadratic difference from unity of the ratio is extracted from the distribution and quoted as an additional systematic uncertainty on the luminosity measurement, to be combined with the visible cross section uncertainty.

Table 4 summarises the uncertainties affecting the T0- and V0-based luminosity measurements. The total luminosity uncertainty ranges from 1.8% to 2.7% depending on the year and luminometer. The table also reports our assessment of which uncertainties are correlated across the three years.

The actual luminosity uncertainty for the combined 2016+2017+2018 sample obviously depends on the exact amount of luminosity used for each year. In order to give the reader a feeling of the size of the uncertainty, we study the case of the analysis reported in Ref. [35]. The integrated luminosity of the used sample, measured with V0, is $(8.12 \pm 0.16)$ nb$^{-1}$ for 2016, $(10.67 \pm 0.29)$ nb$^{-1}$ for 2017, and $(13.14 \pm 0.27)$ nb$^{-1}$ for 2018. The luminosity uncertainty for the combined sample, evaluated by taking into account the correlations reported in Table 4, is 1.6%.

## 4 Conclusions

The ALICE luminosity determination for pp collisions at $\sqrt{s}$ = 13 TeV collected in 2016, 2017 and 2018 uses the results of three van der Meer scans, one per year, where visible cross sections were measured for two reference processes, based on the T0 (with pseudorapidity coverage $4.6 < \eta < 4.9$, $-3.3 < \eta < -3.0$) and V0 ($2.8 < \eta < 5.1$, $-3.7 < \eta < -1.7$) detectors. The stability and consistency of the luminosity measurements based on such visible cross sections have been studied for the full data sample. The obtained luminosity uncertainty ranges from 1.8% to 2.7% depending on the year and luminometer. The luminosity uncertainty for the combined 2016+2017+2018 sample is typically better than 2%.

**Table 4:** Relative uncertainties on the measurement of visible cross sections and luminosity in pp collisions at $\sqrt{s} = 13$ TeV.

| Uncertainty | 2016 | 2017 | 2018 | Correlated? |
|---|---|---|---|---|
| | T0 ǀ V0 | T0 ǀ V0 | T0 ǀ V0 | |
| Statistical | 0.05% ǀ 0.05% | 0.07% ǀ 0.07% | 0.05% ǀ 0.05% | No |
| Bunch intensity | | | | |
| Beam current normalisation | 0.5% | 0.5% | 0.4% | Yes |
| Relative bunch populations | 0.1% | 0.3% | 0.1% | No |
| Ghost and satellite charge | < 0.1% | < 0.1% | < 0.1% | No |
| Non-factorisation | 0.5% | 0.2% | 0.4% | Yes |
| Length-scale calibration | 0.2% | 0.3% | 0.3% | No |
| Beam-beam effects | 0.3% | 0.3% | 0.3% | Yes |
| Orbit drift | 0.1% | 0.1% | 0.2% | No |
| Magnetic non-linearities | 0.1% | 0.2% | 0.2% | Yes |
| Beam centring | < 0.1% | < 0.1% | 0.1% | No |
| Luminosity decay | 0.5% | 0.5% | 0.3% | No |
| Background subtraction | 0.1% ǀ 0.6% | 0.1% ǀ 0.8% | 0.1% ǀ 0.7% | Yes |
| Pile-up | 0.1% ǀ < 0.1% | 0.5% | 0.2% ǀ < 0.1% | Yes |
| Fit model | 0.2% | 0.6% | 0.4% | Yes |
| $h_x h_y$ consistency (T0 vs V0) | 0.1% | 0.4% | 0.4% | No |
| Bunch-by-bunch consistency | < 0.1% ǀ < 0.1% | 0.1% ǀ 0.1% | 0.1% ǀ 0.1% | No |
| Scan-to-scan consistency | 0.2% ǀ 0.1% | 0.1% ǀ 0.1% | 0.5% ǀ 0.5% | No |
| Stability and consistency | 1.5% | 2.3% | 1.6% | No |
| Total correlated | 0.8% ǀ 1.0% | 1.0% ǀ 1.2% | 0.8% ǀ 1.0% | Yes |
| Total uncorrelated | 1.6% ǀ 1.6% | 2.4% ǀ 2.4% | 1.8% ǀ 1.8% | No |
| Total | 1.8% ǀ 1.9% | 2.6% ǀ 2.7% | 1.9% ǀ 2.1% | Partially |

## Acknowledgements

The ALICE Collaboration would like to thank all its engineers and technicians for their invaluable contributions to the construction of the experiment and the CERN accelerator teams for the outstanding performance of the LHC complex. The ALICE Collaboration gratefully acknowledges the resources and support provided by all Grid centres and the Worldwide LHC Computing Grid (WLCG) collaboration. The ALICE Collaboration acknowledges the following funding agencies for their support in building and running the ALICE detector: A. I. Alikhanyan National Science Laboratory (Yerevan Physics Institute) Foundation (ANSL), State Committee of Science and World Federation of Scientists (WFS), Armenia; Austrian Academy of Sciences, Austrian Science Fund (FWF): [M 2467-N36] and Nationalstiftung für Forschung, Technologie und Entwicklung, Austria; Ministry of Communications and High Technologies, National Nuclear Research Center, Azerbaijan; Conselho Nacional de Desenvolvimento Científico e Tecnológico (CNPq), Financiadora de Estudos e Projetos (Finep), Fundação de Amparo à Pesquisa do Estado de São Paulo (FAPESP) and Universidade Federal do Rio Grande do Sul (UFRGS), Brazil; Ministry of Education of China (MOEC) , Ministry of Science & Technology of China (MSTC) and National Natural Science Foundation of China (NSFC), China; Ministry of Science and Education and Croatian Science Foundation, Croatia; Centro de Aplicaciones Tecnológicas y Desarrollo Nuclear (CEADEN), Cubaenergía, Cuba; Ministry of Education, Youth and Sports of the Czech Republic, Czech Republic; The Danish Council for Independent Research | Natural Sciences, the VILLUM FONDEN and Danish National Research Foundation (DNRF), Denmark; Helsinki Institute of Physics (HIP), Finland; Commissariat à l'Energie Atomique (CEA) and Institut National de Physique Nucléaire et de Physique des Particules (IN2P3) and Centre National de la Recherche Scientifique (CNRS), France; Bundesministerium für Bildung und Forschung (BMBF) and GSI Helmholtzzentrum für Schwerionenforschung GmbH, Germany; General Secretariat for Research and Technology, Ministry of Education, Research and Religions, Greece; National Research, Development and Innovation Office, Hungary; Department of Atomic Energy Government of India (DAE), Department of Science and Technology, Government of India (DST), University Grants Commission, Government of India (UGC) and Council of Scientific and Industrial Research (CSIR), India; Indonesian Institute of Science, Indonesia; Istituto Nazionale di Fisica Nucleare (INFN), Italy; Institute for Innovative Science and Technology , Nagasaki Institute of Applied Science (IIST), Japanese Ministry of Education, Culture, Sports, Science and Technology (MEXT) and Japan Society for the Promotion of Science (JSPS) KAKENHI, Japan; Consejo Nacional de Ciencia (CONACYT) y Tecnología, through Fondo de Cooperación Internacional en Ciencia y Tecnología (FONCICYT) and Dirección General de Asuntos del Personal Academico (DGAPA), Mexico; Nederlandse Organisatie voor Wetenschappelijk Onderzoek (NWO), Netherlands; The Research Council of Norway, Norway; Commission on Science and Technology for Sustainable Development in the South (COMSATS), Pakistan; Pontificia Universidad Católica del Perú, Peru; Ministry of Education and Science, National Science Centre and WUT ID-UB, Poland; Korea Institute of Science and Technology Information and National Research Foundation of Korea (NRF), Republic of Korea; Ministry of Education and Scientific Research, Institute of Atomic Physics and Ministry of Research and Innovation and Institute of Atomic Physics, Romania; Joint Institute for Nuclear Research (JINR), Ministry of Education and Science of the Russian Federation, National Research Centre Kurchatov Institute, Russian Science Foundation and Russian Foundation for Basic Research, Russia; Ministry of Education, Science, Research and Sport of the Slovak Republic, Slovakia; National Research Foundation of South Africa, South Africa; Swedish Research Council (VR) and Knut & Alice Wallenberg Foundation (KAW), Sweden; European Organization for Nuclear Research, Switzerland; Suranaree University of Technology (SUT), National Science and Technology Development Agency (NSDTA) and Office of the Higher Education Commission under NRU project of Thailand, Thailand; Turkish Energy, Nuclear and Mineral Research Agency (TENMAK), Turkey; National Academy of Sciences of Ukraine, Ukraine; Science and Technology Facilities Council (STFC), United Kingdom; National Science Foundation of the United States of America (NSF) and United States Department of Energy, Office of Nuclear Physics (DOE NP),

United States of America.

## References


[1] **ALICE** Collaboration, K. Aamodt *et al.*, "The ALICE experiment at the CERN LHC," *JINST* **3** (2008) S08002.

[2] L. Evans and P. Bryant, "LHC Machine," *JINST* **3** (2008) S08001.

[3] S. van der Meer, "Calibration of the effective beam height in the ISR," Tech. Rep. CERN-ISR-PO-68-31, CERN, 1968. http://cds.cern.ch/record/296752.

[4] P. Grafström and W. Kozanecki, "Luminosity determination at proton colliders," *Prog. Part. Nucl. Phys.* **81** (2015) 97–148.

[5] **ATLAS** Collaboration, G. Aad *et al.*, "Luminosity determination in pp collisions at $\sqrt{s}$ = 7 TeV using the ATLAS detector at the LHC," *Eur. Phys. J.* **C71** no. 4, (2011) 1630, arXiv:1101.2185 [hep-ex].

[6] **ATLAS** Collaboration, G. Aad *et al.*, "Improved luminosity determination in pp collisions at $\sqrt{s}$ = 7 TeV using the ATLAS detector at the LHC," *Eur. Phys. J.* **C73** no. 8, (2013) 2518, arXiv:1302.4393 [hep-ex].

[7] **ATLAS** Collaboration, M. Aaboud *et al.*, "Luminosity determination in pp collisions at $\sqrt{s}$ = 8 TeV using the ATLAS detector at the LHC," *Eur. Phys. J.* **C76** no. 12, (2016) 653, arXiv:1608.03953 [hep-ex].

[8] **LHCb** Collaboration, R. Aaij *et al.*, "Absolute luminosity measurements with the LHCb detector at the LHC," *JINST* **7** no. 01, (2012) P01010, arXiv:1110.2866 [hep-ex].

[9] **LHCb** Collaboration, R. Aaij *et al.*, "Precision luminosity measurements at LHCb," *JINST* **9** no. 12, (2014) P12005, arXiv:1410.0149 [hep-ex].

[10] **ALICE** Collaboration, B. Abelev *et al.*, "Measurement of inelastic, single- and double-diffraction cross sections in proton–proton collisions at the LHC with ALICE," *Eur. Phys. J.* **C73** no. 6, (2013) 2456, arXiv:1208.4968 [hep-ex].

[11] **ALICE** Collaboration, B. Abelev *et al.*, "Measurement of visible cross sections in proton-lead collisions at $\sqrt{s_{\rm NN}}$ = 5.02 TeV in van der Meer scans with the ALICE detector," *JINST* **9** no. 11, (2014) P11003, arXiv:1405.1849 [nucl-ex].

[12] **CMS** Collaboration, A. M. Sirunyan *et al.*, "Precision luminosity measurement in proton-proton collisions at $\sqrt{s} = 13$ TeV in 2015 and 2016 at CMS," arXiv:2104.01927 [hep-ex].

[13] **ALICE** Collaboration, J. Adam *et al.*, "ALICE luminosity determination for pp collisions at $\sqrt{s} = 13$ TeV," Tech. Rep. ALICE-PUBLIC-2016-002, CERN, 2016. https://cds.cern.ch/record/2160174/.

[14] **ALICE** Collaboration, S. Acharya *et al.*, "ALICE luminosity determination for pp collisions at $\sqrt{s} = 8$ TeV," Tech. Rep. ALICE-PUBLIC-2017-002, CERN, 2017. https://cds.cern.ch/record/2255216/.

[15] **ALICE** Collaboration, J. Adam *et al.*, "ALICE luminosity determination for pp collisions at $\sqrt{s} = 5$ TeV," Tech. Rep. ALICE-PUBLIC-2016-005, CERN, 2016. https://cds.cern.ch/record/2202638/.

[16] **ALICE** Collaboration, S. Acharya *et al.*, "ALICE 2017 luminosity determination for pp collisions at $\sqrt{s}$ = 5 TeV," Tech. Rep. ALICE-PUBLIC-2018-014, CERN, 2018. https://cds.cern.ch/record/2648933/.

[17] **ALICE** Collaboration, S. Acharya *et al.*, "ALICE luminosity determination for p-Pb collisions at $\sqrt{s_{\rm NN}}$ = 8.16 TeV," Tech. Rep. ALICE-PUBLIC-2018-002, CERN, 2018. https://cds.cern.ch/record/2314660/.

[18] **CMS** Collaboration, "CMS Luminosity Based on Pixel Cluster Counting - Summer 2013 Update," Tech. Rep. CMS-PAS-LUM-13-001, CERN, 2013. https://cds.cern.ch/record/1598864.

[19] **ALICE** Collaboration, B. Abelev *et al.*, "Performance of the ALICE Experiment at the CERN LHC," *Int. J. Mod. Phys.* **A29** (2014) 1430044, arXiv:1402.4476 [nucl-ex].

[20] **ALICE T0 and V0** Collaboration, T. Malkiewicz *et al.*, "Luminosity determination in ALICE with T0 and V0 detectors," *Indian J. Phys.* **85** (2011) 965–970.

[21] **ALICE** Collaboration, E. Abbas *et al.*, "Performance of the ALICE VZERO system," *JINST* **8** (2013) P10016, arXiv:1306.3130 [nucl-ex].

[22] **ALICE** Collaboration, K. Aamodt *et al.*, "Alignment of the ALICE Inner Tracking System with cosmic-ray tracks," *JINST* **5** (2010) P03003, arXiv:1001.0502 [physics.ins-det].

[23] J. J. Gras, D. Belohrad, M. Ludwig, P. Odier, and C. Barschel, "Optimization of the LHC beam current transformers for accurate luminosity determination," Tech. Rep. CERN-ATS-2011-063, CERN, 2011. http://cds.cern.ch/record/1379466.

[24] C. Ohm and T. Pauly, "The ATLAS beam pick-up based timing system," *Nucl. Instrum. Meth.* **A623** (2010) 558–560, arXiv:0905.3648 [physics.ins-det].

[25] A. Alici *et al.*, "Study of the LHC ghost charge and satellite bunches for luminosity calibration.," Tech. Rep. CERN-ATS-Note-2012-029 PERF, CERN, 2012. https://cds.cern.ch/record/1427728.

[26] A. Boccardi, E. Bravin, M. Ferro-Luzzi, S. Mazzoni, and M. Palm, "LHC Luminosity calibration using the Longitudinal Density Monitor," Tech. Rep. CERN-ATS-Note-2013-034 TECH, CERN, 2013. https://cds.cern.ch/record/1556087.

[27] G. Coombs, M. Ferro-Luzzi, and R. Matev, "Beam-Gas Imaging Measurements at LHCb," in *7th International Beam Instrumentation Conference*, p. WEBP13. September, 2018. https://cds.cern.ch/record/2716029.

[28] D. Bishop, C. Boccard, E. Calvo-Giraldo, D. Cocq, L. Jensen, R. Jones, J. J. Savioz, and G. Waters, "The LHC Orbit and Trajectory System," Tech. Rep. CERN-AB-2003-057-BDI, 2003. https://cds.cern.ch/record/624190.

[29] J. Wenninger, "Dispersion Free Steering for YASP and dispersion correction for TI8," Tech. Rep. LHC-Performance-Note-005, CERN, 2009. http://cds.cern.ch/record/1156142.

[30] W. Kozanecki, T. Pieloni, and J. Wenninger, "Observation of Beam-beam Deflections with LHC Orbit Data," Tech. Rep. CERN-ACC-NOTE-2013-0006, CERN, 2013. https://cds.cern.ch/record/1581723.

[31] V. Balagura, "Van der Meer scan luminosity measurement and beam–beam correction," *Eur. Phys. J. C* **81** no. 1, (2021) 26, arXiv:2012.07752 [hep-ex].

[32] S. N. Webb, *Factorisation of beams in van der Meer scans and measurements of the $\phi^*_\eta$ distribution of $Z \to e^+e^-$ events in pp collisions at $\sqrt{s} = 8$ TeV with the ATLAS detector*. PhD thesis, Manchester U., 2015-06-01. https://inspirehep.net/record/1381312/files/CERN-THESIS-2015-054.pdf.

[33] **ATLAS** Collaboration, "Characterization of Interaction-Point Beam Parameters Using the pp Event-Vertex Distribution Reconstructed in the ATLAS Detector at the LHC," Tech. Rep. ATLAS-CONF-2010-027, CERN, 2010. https://cds.cern.ch/record/1277659.

[34] C. Barschel, M. Ferro-Luzzi, J.-J. Gras, M. Ludwig, P. Odier, and S. Thoulet, "Results of the LHC DCCT Calibration Studies," Tech. Rep. CERN-ATS-Note-2012-026 PERF, CERN, 2012. https://cds.cern.ch/record/1425904.

[35] **ALICE** Collaboration, S. Acharya *et al.*, "Measurement of prompt $D^0$, $\Lambda_c^+$, and $\Sigma_c^{0,++}(2455)$ production in pp collisions at $\sqrt{s} = 13$ TeV," arXiv:2106.08278 [hep-ex].

## A The ALICE Collaboration

S. Acharya[143], D. Adamová[98], A. Adler[76], G. Aglieri Rinella[35], M. Agnello[31], N. Agrawal[55], Z. Ahammed[143], S. Ahmad[16], S.U. Ahn[78], I. Ahuja[39], Z. Akbar[52], A. Akindinov[95], M. Al-Turany[110], S.N. Alam[16,41], D. Aleksandrov[91], B. Alessandro[61], H.M. Alfanda[7], R. Alfaro Molina[73], B. Ali[16], Y. Ali[14], A. Alici[26], N. Alizadehvandchali[127], A. Alkin[35], J. Alme[21], T. Alt[70], L. Altenkamper[21], I. Altsybeev[115], M.N. Anaam[7], C. Andrei[49], D. Andreou[93], A. Andronic[146], M. Angeletti[35], V. Anguelov[107], F. Antinori[58], P. Antonioli[55], C. Anuj[16], N. Apadula[82], L. Aphecetche[117], H. Appelshäuser[70], S. Arcelli[26], R. Arnaldi[61], I.C. Arsene[20], M. Arslandok[148,107], A. Augustinus[35], R. Averbeck[110], S. Aziz[80], M.D. Azmi[16], A. Badalà[57], Y.W. Baek[42], X. Bai[131,110], R. Bailhache[70], Y. Bailung[51], R. Bala[104], A. Balbino[31], A. Baldisseri[140], B. Balis[2], M. Ball[44], D. Banerjee[4], R. Barbera[27], L. Barioglio[108], M. Barlou[87], G.G. Barnaföldi[147], L.S. Barnby[97], V. Barret[137], C. Bartels[130], K. Barth[35], E. Bartsch[70], F. Baruffaldi[28], N. Bastid[137], S. Basu[83], G. Batigne[117], B. Batyunya[77], D. Bauri[50], J.L. Bazo Alba[114], I.G. Bearden[92], C. Beattie[148], I. Belikov[139], A.D.C. Bell Hechavarria[146], F. Bellini[26], R. Bellwied[127], S. Belokurova[115], V. Belyaev[96], G. Bencedi[71], S. Beole[25], A. Bercuci[49], Y. Berdnikov[101], A. Berdnikova[107], L. Bergmann[107], M.G. Besoiu[69], L. Betev[35], P.P. Bhaduri[143], A. Bhasin[104], I.R. Bhat[104], M.A. Bhat[4], B. Bhattacharjee[43], P. Bhattacharya[23], L. Bianchi[25], N. Bianchi[53], J. Bielčík[38], J. Bielčíková[98], J. Biernat[120], A. Bilandzic[108], G. Biro[147], S. Biswas[4], J.T. Blair[121], D. Blau[91,84], M.B. Blidaru[110], C. Blume[70], G. Boca[29,59], F. Bock[99], A. Bogdanov[96], S. Boi[23], J. Bok[63], L. Boldizsár[147], A. Bolozdynya[96], M. Bombara[39], P.M. Bond[35], G. Bonomi[142,59], H. Borel[140], A. Borissov[84], H. Bossi[148], E. Botta[25], L. Bratrud[70], P. Braun-Munzinger[110], M. Bregant[123], M. Broz[38], G.E. Bruno[109,34], M.D. Buckland[130], D. Budnikov[111], H. Buesching[70], S. Bufalino[31], O. Bugnon[117], P. Buhler[116], Z. Buthelezi[74,134], J.B. Butt[14], A. Bylinkin[129], S.A. Bysiak[120], M. Cai[28,7], H. Caines[148], A. Caliva[110], E. Calvo Villar[114], J.M.M. Camacho[122], R.S. Camacho[46], P. Camerini[24], F.D.M. Canedo[123], F. Carnesecchi[35,26], R. Caron[140], J. Castillo Castellanos[140], E.A.R. Casula[23], F. Catalano[31], C. Ceballos Sanchez[77], P. Chakraborty[50], S. Chandra[143], S. Chapeland[35], M. Chartier[130], S. Chattopadhyay[143], S. Chattopadhyay[112], A. Chauvin[23], T.G. Chavez[46], T. Cheng[7], C. Cheshkov[138], B. Cheynis[138], V. Chibante Barroso[35], D.D. Chinellato[124], S. Cho[63], P. Chochula[35], P. Christakoglou[93], C.H. Christensen[92], P. Christiansen[83], T. Chujo[136], C. Cicalo[56], L. Cifarelli[26], F. Cindolo[55], M.R. Ciupek[110], G. Clai[II,55], J. Cleymans[I,126], F. Colamaria[54], J.S. Colburn[113], D. Colella[109,54,34,147], A. Collu[82], M. Colocci[35], M. Concas[III,61], G. Conesa Balbastre[81], Z. Conesa del Valle[80], G. Contin[24], J.G. Contreras[38], M.L. Coquet[140], T.M. Cormier[99], P. Cortese[32], M.R. Cosentino[125], F. Costa[35], S. Costanza[29,59], P. Crochet[137], R. Cruz-Torres[82], E. Cuautle[71], P. Cui[7], L. Cunqueiro[99], A. Dainese[58], M.C. Danisch[107], A. Danu[69], I. Das[112], P. Das[89], P. Das[4], S. Das[4], S. Dash[50], S. De[89], A. De Caro[30], G. de Cataldo[54], L. De Cilladi[25], J. de Cuveland[40], A. De Falco[23], D. De Gruttola[30], N. De Marco[61], C. De Martin[24], S. De Pasquale[30], S. Deb[51], H.F. Degenhardt[123], K.R. Deja[144], L. Dello Stritto[30], S. Delsanto[25], W. Deng[7], P. Dhankher[19], D. Di Bari[34], A. Di Mauro[35], R.A. Diaz[8], T. Dietel[126], Y. Ding[138,7], R. Divià[35], D.U. Dixit[19], Ø. Djuvsland[21], U. Dmitrieva[65], J. Do[63], A. Dobrin[69], B. Dönigus[70], O. Dordic[20], A.K. Dubey[143], A. Dubla[110,93], S. Dudi[103], M. Dukhishyam[89], P. Dupieux[137], N. Dzalaiova[13], T.M. Eder[146], R.J. Ehlers[99], V.N. Eikeland[21], F. Eisenhut[70], D. Elia[54], B. Erazmus[117], F. Ercolessi[26], F. Erhardt[102], A. Erokhin[115], M.R. Ersdal[21], B. Espagnon[80], G. Eulisse[35], D. Evans[113], S. Evdokimov[94], L. Fabbietti[108], M. Faggin[28], J. Faivre[81], F. Fan[7], A. Fantoni[53], M. Fasel[99], P. Fecchio[31], A. Feliciello[61], G. Feofilov[115], A. Fernández Téllez[46], A. Ferrero[140], A. Ferretti[25], V.J.G. Feuillard[107], J. Figiel[120], S. Filchagin[111], D. Finogeev[65], F.M. Fionda[56,21], G. Fiorenza[35,109], F. Flor[127], A.N. Flores[121], S. Foertsch[74], P. Foka[110], S. Fokin[91], E. Fragiacomo[62], E. Frajna[147], U. Fuchs[35], N. Funicello[30], C. Furget[81], A. Furs[65], J.J. Gaardhøje[92], M. Gagliardi[25], A.M. Gago[114], A. Gal[139], C.D. Galvan[122], P. Ganoti[87], C. Garabatos[110], J.R.A. Garcia[46], E. Garcia-Solis[10], K. Garg[117], C. Gargiulo[35], A. Garibli[90], K. Garner[146], P. Gasik[110], E.F. Gauger[121], A. Gautam[129], M.B. Gay Ducati[72], M. Germain[117], P. Ghosh[143], S.K. Ghosh[4], M. Giacalone[26], P. Gianotti[53], P. Giubellino[110,61], P. Giubilato[28], A.M.C. Glaenzer[140], P. Glässel[107], D.J.Q. Goh[85], V. Gonzalez[145], L.H. González-Trueba[73], S. Gorbunov[40], M. Gorgon[2], L. Görlich[120], S. Gotovac[36], V. Grabski[73], L.K. Graczykowski[144], L. Greiner[82], A. Grelli[64], C. Grigoras[35], V. Grigoriev[96], S. Grigoryan[77,1], O.S. Groettvik[21], F. Grosa[35,61], J.F. Grosse-Oetringhaus[35], R. Grosso[110], G.G. Guardiano[124], R. Guernane[81], M. Guilbaud[117], K. Gulbrandsen[92], T. Gunji[135], W. Guo[7], A. Gupta[104], R. Gupta[104], S.P. Guzman[46], L. Gyulai[147], M.K. Habib[110], C. Hadjidakis[80], G. Halimoglu[70], H. Hamagaki[85], G. Hamar[147], M. Hamid[7], R. Hannigan[121], M.R. Haque[144,89], A. Harlenderova[110], J.W. Harris[148], A. Harton[10], J.A. Hasenbichler[35], H. Hassan[99], D. Hatzifotiadou[55], P. Hauer[44], L.B. Havener[148], S. Hayashi[135], S.T. Heckel[108], E. Hellbär[110], H. Helstrup[37], T. Herman[38], E.G. Hernandez[46], G. Herrera Corral[9], F. Herrmann[146], K.F. Hetland[37], H. Hillemanns[35], C. Hills[130], B. Hippolyte[139], B. Hofman[64], B. Hohlweger[93], J. Honermann[146], G.H. Hong[149], D. Horak[38], S. Hornung[110], A. Horzyk[2], R. Hosokawa[15], Y. Hou[7], P. Hristov[35], C. Hughes[133], P. Huhn[70], T.J. Humanic[100], H. Hushnud[112], L.A. Husova[146], A. Hutson[127], D. Hutter[40], J.P. Iddon[35,130], R. Ilkaev[111], H. Ilyas[14], M. Inaba[136],

G.M. Innocenti[35], M. Ippolitov[91], A. Isakov[38,98], M.S. Islam[112], M. Ivanov[110], V. Ivanov[101], V. Izucheev[94], M. Jablonski[2], B. Jacak[82], N. Jacazio[35], P.M. Jacobs[82], S. Jadlovska[119], J. Jadlovsky[119], S. Jaelani[64], C. Jahnke[124,123], M.J. Jakubowska[144], A. Jalotra[104], M.A. Janik[144], T. Janson[76], M. Jercic[102], O. Jevons[113], A.A.P. Jimenez[71], F. Jonas[99,146], P.G. Jones[113], J.M. Jowett [35,110], J. Jung[70], M. Jung[70], A. Junique[35], A. Jusko[113], J. Kaewjai[118], P. Kalinak[66], A. Kalweit[35], V. Kaplin[96], S. Kar[7], A. Karasu Uysal[79], D. Karatovic[102], O. Karavichev[65], T. Karavicheva[65], P. Karczmarczyk[144], E. Karpechev[65], A. Kazantsev[91], U. Kebschull[76], R. Keidel[48], D.L.D. Keijdener[64], M. Keil[35], B. Ketzer[44], Z. Khabanova[93], A.M. Khan[7], S. Khan[16], A. Khanzadeev[101], Y. Kharlov[94,84], A. Khatun[16], A. Khuntia[120], B. Kileng[37], B. Kim[17,63], C. Kim[17], D.J. Kim[128], E.J. Kim[75], J. Kim[149], J.S. Kim[42], J. Kim[107], J. Kim[149], J. Kim[75], M. Kim[107], S. Kim[18], T. Kim[149], S. Kirsch[70], I. Kisel[40], S. Kiselev[95], A. Kisiel[144], J.P. Kitowski[2], J.L. Klay[6], J. Klein[35], S. Klein[82], C. Klein-Bösing[146], M. Kleiner[70], T. Klemenz[108], A. Kluge[35], A.G. Knospe[127], C. Kobdaj[118], M.K. Köhler[107], T. Kollegger[110], A. Kondratyev[77], N. Kondratyeva[96], E. Kondratyuk[94], J. Konig[70], S.A. Konigstorfer[108], P.J. Konopka[35,2], G. Kornakov[144], S.D. Koryciak[2], L. Koska[119], A. Kotliarov[98], O. Kovalenko[88], V. Kovalenko[115], M. Kowalski[120], I. Králik[66], A. Kravčáková[39], L. Kreis[110], M. Krivda[113,66], F. Krizek[98], K. Krizkova Gajdosova[38], M. Kroesen[107], M. Krüger[70], E. Kryshen[101], M. Krzewicki[40], V. Kučera[35], C. Kuhn[139], P.G. Kuijer[93], T. Kumaoka[136], D. Kumar[143], L. Kumar[103], N. Kumar[103], S. Kundu[35], P. Kurashvili[88], A. Kurepin[65], A.B. Kurepin[65], A. Kuryakin[111], S. Kushpil[98], J. Kvapil[113], M.J. Kweon[63], J.Y. Kwon[63], Y. Kwon[149], S.L. La Pointe[40], P. La Rocca[27], Y.S. Lai[82], A. Lakrathok[118], M. Lamanna[35], R. Langoy[132], K. Lapidus[35], P. Larionov[35,53], E. Laudi[35], L. Lautner[35,108], R. Lavicka[38], T. Lazareva[115], R. Lea[142,24,59], J. Lehrbach[40], R.C. Lemmon[97], I. León Monzón[122], E.D. Lesser[19], M. Lettrich[35,108], P. Lévai[147], X. Li[11], X.L. Li[7], J. Lien[132], R. Lietava[113], B. Lim[17], S.H. Lim[17], V. Lindenstruth[40], A. Lindner[49], C. Lippmann[110], A. Liu[19], D.H. Liu[7], J. Liu[130], I.M. Lofnes[21], V. Loginov[96], C. Loizides[99], P. Loncar[36], J.A. Lopez[107], X. Lopez[137], E. López Torres[8], J.R. Luhder[146], M. Lunardon[28], G. Luparello[62], Y.G. Ma[41], A. Maevskaya[65], M. Mager[35], T. Mahmoud[44], A. Maire[139], M. Malaev[101], N.M. Malik[104], Q.W. Malik[20], L. Malinina[IV,77], D. Mal'Kevich[95], N. Mallick[51], P. Malzacher[110], G. Mandaglio[33,57], V. Manko[91], F. Manso[137], V. Manzari[54], Y. Mao[7], J. Mareš[68], G.V. Margagliotti[24], A. Margotti[55], A. Marín[110], C. Markert[121], M. Marquard[70], N.A. Martin[107], P. Martinengo[35], J.L. Martinez[127], M.I. Martínez[46], G. Martínez García[117], S. Masciocchi[110], M. Masera[25], A. Masoni[56], L. Massacrier[80], A. Mastroserio[141,54], A.M. Mathis[108], O. Matonoha[83], P.F.T. Matuoka[123], A. Matyja[120], C. Mayer[120], A.L. Mazuecos[35], F. Mazzaschi[25], M. Mazzilli[35], M.A. Mazzoni[I,60], J.E. Mdhluli[134], A.F. Mechler[70], F. Meddi[22], Y. Melikyan[65], A. Menchaca-Rocha[73], E. Meninno[116,30], A.S. Menon[127], M. Meres[13], S. Mhlanga[126,74], Y. Miake[136], L. Micheletti[61,25], L.C. Migliorin[138], D.L. Mihaylov[108], K. Mikhaylov[77,95], A.N. Mishra[147], D. Miśkowiec[110], A. Modak[4], A.P. Mohanty[64], B. Mohanty[89], M. Mohisin Khan[V,16], M.A. Molander[45], Z. Moravcova[92], C. Mordasini[108], D.A. Moreira De Godoy[146], L.A.P. Moreno[46], I. Morozov[65], A. Morsch[35], T. Mrnjavac[35], V. Muccifora[53], E. Mudnic[36], D. Mühlheim[146], S. Muhuri[143], J.D. Mulligan[82], A. Mulliri[23], M.G. Munhoz[123], R.H. Munzer[70], H. Murakami[135], S. Murray[126], L. Musa[35], J. Musinsky[66], J.W. Myrcha[144], B. Naik[134,50], R. Nair[88], B.K. Nandi[50], R. Nania[55], E. Nappi[54], A.F. Nassirpour[83], A. Nath[107], C. Nattrass[133], A. Neagu[20], L. Nellen[71], S.V. Nesbo[37], G. Neskovic[40], D. Nesterov[115], B.S. Nielsen[92], S. Nikolaev[91], S. Nikulin[91], V. Nikulin[101], F. Noferini[55], S. Noh[12], P. Nomokonov[77], J. Norman[130], N. Novitzky[136], P. Nowakowski[144], A. Nyanin[91], J. Nystrand[21], M. Ogino[85], A. Ohlson[83], V.A. Okorokov[96], J. Oleniacz[144], A.C. Oliveira Da Silva[133], M.H. Oliver[148], A. Onnerstad[128], C. Oppedisano[61], A. Ortiz Velasquez[71], T. Osako[47], A. Oskarsson[83], J. Otwinowski[120], M. Oya[47], K. Oyama[85], Y. Pachmayer[107], S. Padhan[50], D. Pagano[142,59], G. Paić[71], A. Palasciano[54], J. Pan[145], S. Panebianco[140], P. Pareek[143], J. Park[63], J.E. Parkkila[128], S.P. Pathak[127], R.N. Patra[104,35], B. Paul[23], H. Pei[7], T. Peitzmann[64], X. Peng[7], L.G. Pereira[72], H. Pereira Da Costa[140], D. Peresunko[91,84], G.M. Perez[8], S. Perrin[140], Y. Pestov[5], V. Petráček[38], M. Petrovici[49], R.P. Pezzi[117,72], S. Piano[62], M. Pikna[13], P. Pillot[117], O. Pinazza[55,35], L. Pinsky[127], C. Pinto[27], S. Pisano[53], M. Płoskoń[82], M. Planinic[102], F. Pliquett[70], M.G. Poghosyan[99], B. Polichtchouk[94], S. Politano[31], N. Poljak[102], A. Pop[49], S. Porteboeuf-Houssais[137], J. Porter[82], V. Pozdniakov[77], S.K. Prasad[4], R. Preghenella[55], F. Prino[61], C.A. Pruneau[145], I. Pshenichnov[65], M. Puccio[35], S. Qiu[93], L. Quaglia[25], R.E. Quishpe[127], S. Ragoni[113], A. Rakotozafindrabe[140], L. Ramello[32], F. Rami[139], S.A.R. Ramirez[46], A.G.T. Ramos[34], T.A. Rancien[81], R. Raniwala[105], S. Raniwala[105], S.S. Räsänen[45], R. Rath[51], I. Ravasenga[93], K.F. Read[99,133], A.R. Redelbach[40], K. Redlich[VI,88], A. Rehman[21], P. Reichelt[70], F. Reidt[35], H.A. Reme-ness[37], R. Renfordt[70], Z. Rescakova[39], K. Reygers[107], A. Riabov[101], V. Riabov[101], T. Richert[83], M. Richter[20], W. Riegler[35], F. Riggi[27], C. Ristea[69], M. Rodríguez Cahuantzi[46], K. Røed[20], R. Rogalev[94], E. Rogochaya[77], T.S. Rogoschinski[70], D. Rohr[35], D. Röhrich[21], P.F. Rojas[46], P.S. Rokita[144], F. Ronchetti[53], A. Rosano[33,57], E.D. Rosas[71], A. Rossi[58], A. Rotondi[29,59], A. Roy[51], P. Roy[112], S. Roy[50], N. Rubini[26], O.V. Rueda[83], R. Rui[24], B. Rumyantsev[77], P.G. Russek[2], A. Rustamov[90], E. Ryabinkin[91], Y. Ryabov[101], A. Rybicki[120], H. Rytkonen[128], W. Rzesa[144],

O.A.M. Saarimaki[45], R. Sadek[117], S. Sadovsky[94], J. Saetre[21], K. Šafařík[38], S.K. Saha[143], S. Saha[89], B. Sahoo[50], P. Sahoo[50], R. Sahoo[51], S. Sahoo[67], D. Sahu[51], P.K. Sahu[67], J. Saini[143], S. Sakai[136], S. Sambyal[104], V. Samsonov[I,101,96], D. Sarkar[145], N. Sarkar[143], P. Sarma[43], V.M. Sarti[108], M.H.P. Sas[148], J. Schambach[99,121], H.S. Scheid[70], C. Schiaua[49], R. Schicker[107], A. Schmah[107], C. Schmidt[110], H.R. Schmidt[106], M.O. Schmidt[35], M. Schmidt[106], N.V. Schmidt[99,70], A.R. Schmier[133], R. Schotter[139], J. Schukraft[35], Y. Schutz[139], K. Schwarz[110], K. Schweda[110], G. Scioli[26], E. Scomparin[61], J.E. Seger[15], Y. Sekiguchi[135], D. Sekihata[135], I. Selyuzhenkov[110,96], S. Senyukov[139], J.J. Seo[63], D. Serebryakov[65], L. Šerkšnytė[108], A. Sevcenco[69], T.J. Shaba[74], A. Shabanov[65], A. Shabetai[117], R. Shahoyan[35], W. Shaikh[112], A. Shangaraev[94], A. Sharma[103], H. Sharma[120], M. Sharma[104], N. Sharma[103], S. Sharma[104], U. Sharma[104], O. Sheibani[127], K. Shigaki[47], M. Shimomura[86], S. Shirinkin[95], Q. Shou[41], Y. Sibiriak[91], S. Siddhanta[56], T. Siemiarczuk[88], T.F. Silva[123], D. Silvermyr[83], T. Simantathammakul[118], G. Simonetti[35], B. Singh[108], R. Singh[89], R. Singh[104], R. Singh[51], V.K. Singh[143], V. Singhal[143], T. Sinha[112], B. Sitar[13], M. Sitta[32], T.B. Skaali[20], G. Skorodumovs[107], M. Slupecki[45], N. Smirnov[148], R.J.M. Snellings[64], C. Soncco[114], J. Song[127], A. Songmoolnak[118], F. Soramel[28], S. Sorensen[133], I. Sputowska[120], J. Stachel[107], I. Stan[69], P.J. Steffanic[133], S.F. Stiefelmaier[107], D. Stocco[117], I. Storehaug[20], M.M. Storetvedt[37], C.P. Stylianidis[93], A.A.P. Suaide[123], T. Sugitate[47], C. Suire[80], M. Sukhanov[65], M. Suljic[35], R. Sultanov[95], M. Šumbera[98], V. Sumberia[104], S. Sumowidagdo[52], S. Swain[67], A. Szabo[13], I. Szarka[13], U. Tabassam[14], S.F. Taghavi[108], G. Taillepied[137], J. Takahashi[124], G.J. Tambave[21], S. Tang[137,7], Z. Tang[131], J.D. Tapia Takaki[VII,129], M. Tarhini[117], M.G. Tarzila[49], A. Tauro[35], G. Tejeda Muñoz[46], A. Telesca[35], L. Terlizzi[25], C. Terrevoli[127], G. Tersimonov[3], S. Thakur[143], D. Thomas[121], R. Tieulent[138], A. Tikhonov[65], A.R. Timmins[127], M. Tkacik[119], A. Toia[70], N. Topilskaya[65], M. Toppi[53], F. Torales-Acosta[19], T. Tork[80], S.R. Torres[38], A. Trifiró[33,57], S. Tripathy[55,71], T. Tripathy[50], S. Trogolo[35,28], V. Trubnikov[3], W.H. Trzaska[128], T.P. Trzcinski[144], B.A. Trzeciak[38], A. Tumkin[111], R. Turrisi[58], T.S. Tveter[20], K. Ullaland[21], A. Uras[138], M. Urioni[59,142], G.L. Usai[23], M. Vala[39], N. Valle[59,29], S. Vallero[61], N. van der Kolk[64], L.V.R. van Doremalen[64], M. van Leeuwen[93], P. Vande Vyvre[35], D. Varga[147], Z. Varga[147], M. Varga-Kofarago[147], A. Vargas[46], M. Vasileiou[87], A. Vasiliev[91], O. Vázquez Doce[53,108], V. Vechernin[115], E. Vercellin[25], S. Vergara Limón[46], L. Vermunt[64], R. Vértesi[147], M. Verweij[64], L. Vickovic[36], Z. Vilakazi[134], O. Villalobos Baillie[113], G. Vino[54], A. Vinogradov[91], T. Virgili[30], V. Vislavicius[92], A. Vodopyanov[77], B. Volkel[35], M.A. Völkl[107], K. Voloshin[95], S.A. Voloshin[145], G. Volpe[34], B. von Haller[35], I. Vorobyev[108], D. Voscek[119], N. Vozniuk[65], J. Vrláková[39], B. Wagner[21], C. Wang[41], D. Wang[41], M. Weber[116], R.J.G.V. Weelden[93], A. Wegrzynek[35], S.C. Wenzel[35], J.P. Wessels[146], J. Wiechula[70], J. Wikne[20], G. Wilk[88], J. Wilkinson[110], G.A. Willems[146], B. Windelband[107], M. Winn[140], W.E. Witt[133], J.R. Wright[121], W. Wu[41], Y. Wu[131], R. Xu[7], A.K. Yadav[143], S. Yalcin[79], Y. Yamaguchi[47], K. Yamakawa[47], S. Yang[21], S. Yano[47], Z. Yin[7], H. Yokoyama[64], I.-K. Yoo[17], J.H. Yoon[63], S. Yuan[21], A. Yuncu[107], V. Zaccolo[24], C. Zampolli[35], H.J.C. Zanoli[64], N. Zardoshti[35], A. Zarochentsev[115], P. Závada[68], N. Zaviyalov[111], M. Zhalov[101], B. Zhang[7], S. Zhang[41], X. Zhang[7], Y. Zhang[131], V. Zherebchevskii[115], Y. Zhi[11], N. Zhigareva[95], D. Zhou[7], Y. Zhou[92], J. Zhu[7,110], Y. Zhu[7], A. Zichichi[26], G. Zinovjev[3], N. Zurlo[142,59]

## Affiliation notes

[I] Deceased
[II] Also at: Italian National Agency for New Technologies, Energy and Sustainable Economic Development (ENEA), Bologna, Italy
[III] Also at: Dipartimento DET del Politecnico di Torino, Turin, Italy
[IV] Also at: M.V. Lomonosov Moscow State University, D.V. Skobeltsyn Institute of Nuclear, Physics, Moscow, Russia
[V] Also at: Department of Applied Physics, Aligarh Muslim University, Aligarh, India
[VI] Also at: Institute of Theoretical Physics, University of Wroclaw, Poland
[VII] Also at: University of Kansas, Lawrence, Kansas, United States

## Collaboration Institutes

[1] A.I. Alikhanyan National Science Laboratory (Yerevan Physics Institute) Foundation, Yerevan, Armenia
[2] AGH University of Science and Technology, Cracow, Poland
[3] Bogolyubov Institute for Theoretical Physics, National Academy of Sciences of Ukraine, Kiev, Ukraine
[4] Bose Institute, Department of Physics and Centre for Astroparticle Physics and Space Science (CAPSS), Kolkata, India

[5] Budker Institute for Nuclear Physics, Novosibirsk, Russia
[6] California Polytechnic State University, San Luis Obispo, California, United States
[7] Central China Normal University, Wuhan, China
[8] Centro de Aplicaciones Tecnológicas y Desarrollo Nuclear (CEADEN), Havana, Cuba
[9] Centro de Investigación y de Estudios Avanzados (CINVESTAV), Mexico City and Mérida, Mexico
[10] Chicago State University, Chicago, Illinois, United States
[11] China Institute of Atomic Energy, Beijing, China
[12] Chungbuk National University, Cheongju, Republic of Korea
[13] Comenius University Bratislava, Faculty of Mathematics, Physics and Informatics, Bratislava, Slovakia
[14] COMSATS University Islamabad, Islamabad, Pakistan
[15] Creighton University, Omaha, Nebraska, United States
[16] Department of Physics, Aligarh Muslim University, Aligarh, India
[17] Department of Physics, Pusan National University, Pusan, Republic of Korea
[18] Department of Physics, Sejong University, Seoul, Republic of Korea
[19] Department of Physics, University of California, Berkeley, California, United States
[20] Department of Physics, University of Oslo, Oslo, Norway
[21] Department of Physics and Technology, University of Bergen, Bergen, Norway
[22] Dipartimento di Fisica dell'Università 'La Sapienza' and Sezione INFN, Rome, Italy
[23] Dipartimento di Fisica dell'Università and Sezione INFN, Cagliari, Italy
[24] Dipartimento di Fisica dell'Università and Sezione INFN, Trieste, Italy
[25] Dipartimento di Fisica dell'Università and Sezione INFN, Turin, Italy
[26] Dipartimento di Fisica e Astronomia dell'Università and Sezione INFN, Bologna, Italy
[27] Dipartimento di Fisica e Astronomia dell'Università and Sezione INFN, Catania, Italy
[28] Dipartimento di Fisica e Astronomia dell'Università and Sezione INFN, Padova, Italy
[29] Dipartimento di Fisica e Nucleare e Teorica, Università di Pavia, Pavia, Italy
[30] Dipartimento di Fisica 'E.R. Caianiello' dell'Università and Gruppo Collegato INFN, Salerno, Italy
[31] Dipartimento DISAT del Politecnico and Sezione INFN, Turin, Italy
[32] Dipartimento di Scienze e Innovazione Tecnologica dell'Università del Piemonte Orientale and INFN Sezione di Torino, Alessandria, Italy
[33] Dipartimento di Scienze MIFT, Università di Messina, Messina, Italy
[34] Dipartimento Interateneo di Fisica 'M. Merlin' and Sezione INFN, Bari, Italy
[35] European Organization for Nuclear Research (CERN), Geneva, Switzerland
[36] Faculty of Electrical Engineering, Mechanical Engineering and Naval Architecture, University of Split, Split, Croatia
[37] Faculty of Engineering and Science, Western Norway University of Applied Sciences, Bergen, Norway
[38] Faculty of Nuclear Sciences and Physical Engineering, Czech Technical University in Prague, Prague, Czech Republic
[39] Faculty of Science, P.J. Šafárik University, Košice, Slovakia
[40] Frankfurt Institute for Advanced Studies, Johann Wolfgang Goethe-Universität Frankfurt, Frankfurt, Germany
[41] Fudan University, Shanghai, China
[42] Gangneung-Wonju National University, Gangneung, Republic of Korea
[43] Gauhati University, Department of Physics, Guwahati, India
[44] Helmholtz-Institut für Strahlen- und Kernphysik, Rheinische Friedrich-Wilhelms-Universität Bonn, Bonn, Germany
[45] Helsinki Institute of Physics (HIP), Helsinki, Finland
[46] High Energy Physics Group, Universidad Autónoma de Puebla, Puebla, Mexico
[47] Hiroshima University, Hiroshima, Japan
[48] Hochschule Worms, Zentrum für Technologietransfer und Telekommunikation (ZTT), Worms, Germany
[49] Horia Hulubei National Institute of Physics and Nuclear Engineering, Bucharest, Romania
[50] Indian Institute of Technology Bombay (IIT), Mumbai, India
[51] Indian Institute of Technology Indore, Indore, India
[52] Indonesian Institute of Sciences, Jakarta, Indonesia
[53] INFN, Laboratori Nazionali di Frascati, Frascati, Italy
[54] INFN, Sezione di Bari, Bari, Italy
[55] INFN, Sezione di Bologna, Bologna, Italy
[56] INFN, Sezione di Cagliari, Cagliari, Italy

[57] INFN, Sezione di Catania, Catania, Italy
[58] INFN, Sezione di Padova, Padova, Italy
[59] INFN, Sezione di Pavia, Pavia, Italy
[60] INFN, Sezione di Roma, Rome, Italy
[61] INFN, Sezione di Torino, Turin, Italy
[62] INFN, Sezione di Trieste, Trieste, Italy
[63] Inha University, Incheon, Republic of Korea
[64] Institute for Gravitational and Subatomic Physics (GRASP), Utrecht University/Nikhef, Utrecht, Netherlands
[65] Institute for Nuclear Research, Academy of Sciences, Moscow, Russia
[66] Institute of Experimental Physics, Slovak Academy of Sciences, Košice, Slovakia
[67] Institute of Physics, Homi Bhabha National Institute, Bhubaneswar, India
[68] Institute of Physics of the Czech Academy of Sciences, Prague, Czech Republic
[69] Institute of Space Science (ISS), Bucharest, Romania
[70] Institut für Kernphysik, Johann Wolfgang Goethe-Universität Frankfurt, Frankfurt, Germany
[71] Instituto de Ciencias Nucleares, Universidad Nacional Autónoma de México, Mexico City, Mexico
[72] Instituto de Física, Universidade Federal do Rio Grande do Sul (UFRGS), Porto Alegre, Brazil
[73] Instituto de Física, Universidad Nacional Autónoma de México, Mexico City, Mexico
[74] iThemba LABS, National Research Foundation, Somerset West, South Africa
[75] Jeonbuk National University, Jeonju, Republic of Korea
[76] Johann-Wolfgang-Goethe Universität Frankfurt Institut für Informatik, Fachbereich Informatik und Mathematik, Frankfurt, Germany
[77] Joint Institute for Nuclear Research (JINR), Dubna, Russia
[78] Korea Institute of Science and Technology Information, Daejeon, Republic of Korea
[79] KTO Karatay University, Konya, Turkey
[80] Laboratoire de Physique des 2 Infinis, Irène Joliot-Curie, Orsay, France
[81] Laboratoire de Physique Subatomique et de Cosmologie, Université Grenoble-Alpes, CNRS-IN2P3, Grenoble, France
[82] Lawrence Berkeley National Laboratory, Berkeley, California, United States
[83] Lund University Department of Physics, Division of Particle Physics, Lund, Sweden
[84] Moscow Institute for Physics and Technology, Moscow, Russia
[85] Nagasaki Institute of Applied Science, Nagasaki, Japan
[86] Nara Women's University (NWU), Nara, Japan
[87] National and Kapodistrian University of Athens, School of Science, Department of Physics , Athens, Greece
[88] National Centre for Nuclear Research, Warsaw, Poland
[89] National Institute of Science Education and Research, Homi Bhabha National Institute, Jatni, India
[90] National Nuclear Research Center, Baku, Azerbaijan
[91] National Research Centre Kurchatov Institute, Moscow, Russia
[92] Niels Bohr Institute, University of Copenhagen, Copenhagen, Denmark
[93] Nikhef, National institute for subatomic physics, Amsterdam, Netherlands
[94] NRC Kurchatov Institute IHEP, Protvino, Russia
[95] NRC «Kurchatov»Institute - ITEP, Moscow, Russia
[96] NRNU Moscow Engineering Physics Institute, Moscow, Russia
[97] Nuclear Physics Group, STFC Daresbury Laboratory, Daresbury, United Kingdom
[98] Nuclear Physics Institute of the Czech Academy of Sciences, Řež u Prahy, Czech Republic
[99] Oak Ridge National Laboratory, Oak Ridge, Tennessee, United States
[100] Ohio State University, Columbus, Ohio, United States
[101] Petersburg Nuclear Physics Institute, Gatchina, Russia
[102] Physics department, Faculty of science, University of Zagreb, Zagreb, Croatia
[103] Physics Department, Panjab University, Chandigarh, India
[104] Physics Department, University of Jammu, Jammu, India
[105] Physics Department, University of Rajasthan, Jaipur, India
[106] Physikalisches Institut, Eberhard-Karls-Universität Tübingen, Tübingen, Germany
[107] Physikalisches Institut, Ruprecht-Karls-Universität Heidelberg, Heidelberg, Germany
[108] Physik Department, Technische Universität München, Munich, Germany
[109] Politecnico di Bari and Sezione INFN, Bari, Italy
[110] Research Division and ExtreMe Matter Institute EMMI, GSI Helmholtzzentrum für Schwerionenforschung

GmbH, Darmstadt, Germany
[111] Russian Federal Nuclear Center (VNIIEF), Sarov, Russia
[112] Saha Institute of Nuclear Physics, Homi Bhabha National Institute, Kolkata, India
[113] School of Physics and Astronomy, University of Birmingham, Birmingham, United Kingdom
[114] Sección Física, Departamento de Ciencias, Pontificia Universidad Católica del Perú, Lima, Peru
[115] St. Petersburg State University, St. Petersburg, Russia
[116] Stefan Meyer Institut für Subatomare Physik (SMI), Vienna, Austria
[117] SUBATECH, IMT Atlantique, Université de Nantes, CNRS-IN2P3, Nantes, France
[118] Suranaree University of Technology, Nakhon Ratchasima, Thailand
[119] Technical University of Košice, Košice, Slovakia
[120] The Henryk Niewodniczanski Institute of Nuclear Physics, Polish Academy of Sciences, Cracow, Poland
[121] The University of Texas at Austin, Austin, Texas, United States
[122] Universidad Autónoma de Sinaloa, Culiacán, Mexico
[123] Universidade de São Paulo (USP), São Paulo, Brazil
[124] Universidade Estadual de Campinas (UNICAMP), Campinas, Brazil
[125] Universidade Federal do ABC, Santo Andre, Brazil
[126] University of Cape Town, Cape Town, South Africa
[127] University of Houston, Houston, Texas, United States
[128] University of Jyväskylä, Jyväskylä, Finland
[129] University of Kansas, Lawrence, Kansas, United States
[130] University of Liverpool, Liverpool, United Kingdom
[131] University of Science and Technology of China, Hefei, China
[132] University of South-Eastern Norway, Tonsberg, Norway
[133] University of Tennessee, Knoxville, Tennessee, United States
[134] University of the Witwatersrand, Johannesburg, South Africa
[135] University of Tokyo, Tokyo, Japan
[136] University of Tsukuba, Tsukuba, Japan
[137] Université Clermont Auvergne, CNRS/IN2P3, LPC, Clermont-Ferrand, France
[138] Université de Lyon, CNRS/IN2P3, Institut de Physique des 2 Infinis de Lyon , Lyon, France
[139] Université de Strasbourg, CNRS, IPHC UMR 7178, F-67000 Strasbourg, France, Strasbourg, France
[140] Université Paris-Saclay Centre d'Etudes de Saclay (CEA), IRFU, Départment de Physique Nucléaire (DPhN), Saclay, France
[141] Università degli Studi di Foggia, Foggia, Italy
[142] Università di Brescia, Brescia, Italy
[143] Variable Energy Cyclotron Centre, Homi Bhabha National Institute, Kolkata, India
[144] Warsaw University of Technology, Warsaw, Poland
[145] Wayne State University, Detroit, Michigan, United States
[146] Westfälische Wilhelms-Universität Münster, Institut für Kernphysik, Münster, Germany
[147] Wigner Research Centre for Physics, Budapest, Hungary
[148] Yale University, New Haven, Connecticut, United States
[149] Yonsei University, Seoul, Republic of Korea